J Mater Sci (2006) 41:7319–7323
DOI 10.1007/s10853-006-0961-3

Defect engineering for high-power 780 nm AlGaAs laser diodes

D. S. Kim · W. C. Choi · G. W. Moon · K. Y. Jang · T. G. Kim · Y. M. Sung

Received: 14 September 2005 / Accepted: 27 December 2005 / Published online: 17 October 2006

Abstract Defect engineering is carried out to determine optimum growth conditions for highly reliable high-power 780 nm AlGaAs laser diodes (LDs) using deep level transient spectroscopy (DLTS). The DLTS results reveal that the defect density of the $Al_{0.48}Ga_{0.52}As$ cladding layer depended heavily on growth temperature and AsH_3 flow but that of the $Al_{0.1}Ga_{0.9}As$ active layer depended mostly on the growth rates of the active layer. As a result of layer optimization at growth condition by DLTS, a record high output power of 250 mW was obtained at an operating current as low as 129.6 mA under room temperature continuous wave (CW) operation.

Introduction

A high-power and high-reliability 780-nm-band laser diode (LD) is an important light source for high-density optical recording systems [1]. This laser diode can achieve continuous wave (CW) operation at more than 100 mW in the fundamental mode; however, there is a demand for much higher output power to increase the data writing and erasing speed of the CD-RW system. One of the significant issues affecting light output power increase is the suppression of local heating at mirror facets of lasers. This local heating due to the self-absorption of light by non-radiative crystal defects causes the sudden degradation of mirror facets called catastrophic optical damage (COD). Many efforts have been devoted to increase the COD power level by using smart laser structures such as the window structure [2] and the buried twin-ridge structure [3]. These structures try to increase the effective energy bandgap of the active layer in the facet region so that the near-field spot size can be expanded at the facet, and thereby, the optical density can be kept below the COD level. The optical power density at the mirror facet can be reduced by using a thin active layer as well [4].

On the other hand, AlGaAs grown by metalorganic chemical vapor deposition (MOCVD) tend to include many oxygen-related deep-level defects because it easily reacts with oxygen (O_2) and tend to include structural defects at high temperature [5]. These deep-level defects increase the threshold current density and reduce the radiative efficiency of the laser to eventually decrease the COD level. In this regard, it is very important to tightly control the distribution and density of such deep-level defects in each layer of a high-power 780-nm-band laser diode to improve the overall laser performance as well as the COD power level. However, conventional techniques such as X-ray and photoluminescence, generally used for achieving optimum growth condition, don not provide precise growth conditions of the device structures.

In this work, deep level transient spectroscopies (DLTS) [6] of both $Al_{0.48}Ga_{0.52}As$ cladding layers and

D. S. Kim · W. C. Choi · T. G. Kim (✉)
Department of Electronic Engineering, Korea University, 5-1, Anam, Sungbuk, Seoul 136-075, Korea
e-mail: tgkim1@korea.ac.kr

G. W. Moon · K. Y. Jang
Discrete Semiconductor Device Division, Samsung Electro-Mechanics, 443-803 Suwon, Korea

Y. M. Sung
Department of Material Science and Engineering, Korea University, 5-1 Anam, Sungbuk, Seoul 136-075, Korea

$Al_{0.1}Ga_{0.9}As$ active layers are measured to find the optimum growth condition for a high-power and high-reliability 780-nm-band AlGaAs laser. Four AlGaAs lasers with different growth parameters are then fabricated to confirm the effect of defect engineering on laser performance. One of the lasers grown according to the DLTS result showed a threshold current of 38 mA and a COD power of 250 mW under room temperature (RT) CW operation.

Experimental procedure

All the samples were grown in the same environment as the full laser structure by a low-pressure MOCVD system on (100)-oriented n^+ GaAs substrate. Trimethylgallium (TMGa) and trimethylauminum (TMAl) and arsine (AsH_3) were used as the sources of Ga, Al, and As, respectively. DEZn was used as the doping source of the p-type layer. The four $Al_{0.48}Ga_{0.52}As$ cladding layers were grown at temperatures of 740 and 790 °C under different AsH_3 flows of 300 and 500 sccm, respectively, and $Al_{0.1}Ga_{0.9}As$ active layers were grown at 790 °C under different growth rates of 7 and 10 Å/s. The doping concentrations obtained from the capacitance–voltage (C–V) measurements were in the order of 7×10^{-17} cm^{-3} for the $Al_{0.48}Ga_{0.52}As$ samples and 1×10^{-17} cm^{-3} for the $Al_{0.1}Ga_{0.9}As$ samples.

The DLTS measurements were carried out by using a completely automated measurement set-up including a HP4120A C-V/C-t meter, an external generator HP8116A, and a gas-flow cryostat of Oxford Instruments. Samples were mounted in a liquid nitrogen bath type sample holder, provided in a heater, to measure the DLTS signals within the 70~400 K temperature range. The DLTS signals were recorded at the input bias of the filling pulse $V = 1$ V, pulse width $W = 1$ ms, and filling duration $t_p = 1$ ms. Trap parameters such as trap density and activation energy were calculated under the following conditions. The amplitude of the DLTS signal is directly related to the trap density N_t by

$$N_t = \frac{(N_A - N_D)2\Delta C}{C_0} \quad (1)$$

where ΔC is the height of the signal peak, C_0 is the sample junction capacitance at the peak temperature, and N_A–N_D is the net acceptor concentration [6]. The activation energy E_a of the trap is determined from the Arrhenius plot of $1/T^2\tau$ versus $1000/T$, and the emission time constant τ is given as

$$\tau = \frac{t_2 - t_1}{\ln(t_2/t_1)} \quad (2)$$

where t_1 and t_2 are gating times.

Results and discussion

Typical DLTS spectra and the Arrhenius plots obtained form four $Al_{0.48}Ga_{0.52}As$ cladding layers are shown in Figs. 1 and 2, respectively. The sample numbers, growth conditions, and physical quantities of the deep-level defects observed in Figs. 1 and 2 are summarized in Table 1. For $Al_{0.48}Ga_{0.52}As$ cladding layers grown at 740 °C, one deep-level signal near 0.88 eV was observed from sample #101 grown at an AsH_3 flow of 300 sccm, and one deep-level signal was detected near 0.63 eV from sample #102 grown at an AsH_3 flow of 500 sccm. In addition, for $Al_{0.48}Ga_{0.52}As$ cladding layers grown at 790 °C, one deep-level signal near 0.58 eV was observed from sample #103 grown at an AsH_3 flow of 300 sccm, and one deep-level signal near 0.61 eV was observed from sample #104 grown at an AsH_3 flow of 500 sccm. The exact origin of these deep-level defects was not identified; however, the deep-level defects near 0.58~0.63 eV were attributed to Ga vancancy-O_2 complexes according to the reference [7]. Oxygen related deep level defects act as non-radiative recombination centers, decreasing the radiative efficiency. In addition, the deep level defects near 0.88 eV are due to the EL2 levels [8]. Among the four samples, sample #103 showed the least trap density for the $Al_{0.48}Ga_{0.52}As$ cladding layer, regardless of the trap origin. Based on the DLTS result, the trap density tended to decrease under relatively higher growth temperature and lower AsH_3 flow.

In the same manner, the typical DLTS spectra and the Arrhenius plots were observed from two $Al_{0.1}Ga_{0.9}As$ samples grown at different grow rates of 7 and 10 Å/s as shown in Figs. 3 and 4, respectively. Based on the

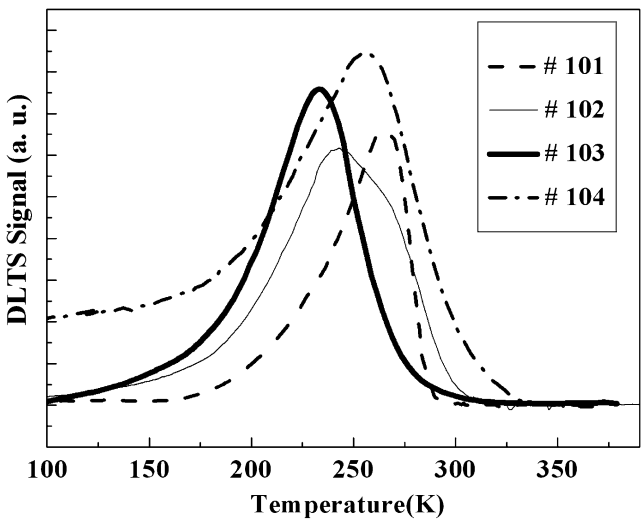

Fig. 1 DLTS spectra of four $Al_{0.48}Ga_{0.52}As$ cladding layers

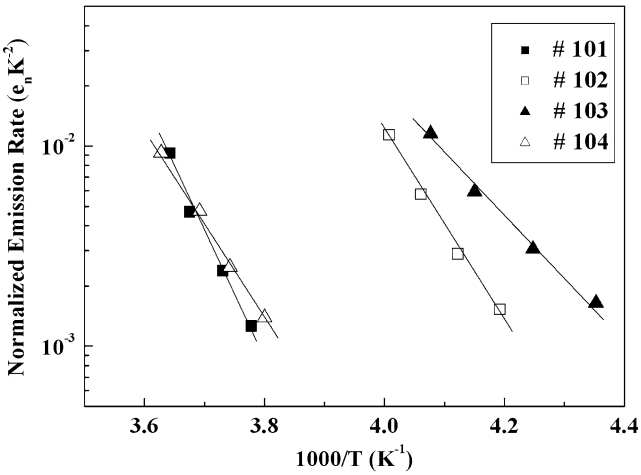

Fig. 2 Arrhenius plots obtained from four $Al_{0.48}Ga_{0.52}As$ cladding layers

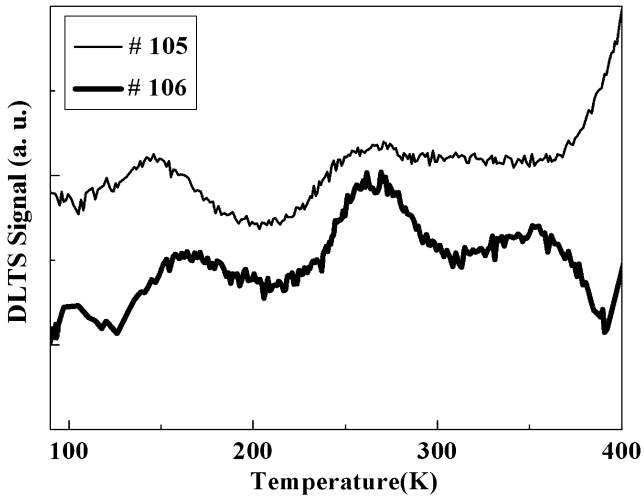

Fig. 3 DLTS spectra measured from two $Al_{0.1}Ga_{0.9}As$ active layers

energetic position, three dominant DLTS signals were observed at about 150, 250 and 350 K for both samples (#105, #106), regardless of the growth rate. The deep-level defects near 0.3 eV, which appeared only in the MOCVD grown epi-layers, did not seem to relate to the DX center since the DX center did not appear for x smaller than 0.2 [9]. In addition, the deep-level defect near 1.0 eV, which appeared in most AlGaAs layers, regardless of the crystal growth technique, was due to intrinsic defects such as isolated interstitials, vacancies, or their binary complexes associated with doping or residual impurities [8]. The comparison of the two samples shows that relatively higher growth rates tended to reduce the trap density of the $Al_{0.1}Ga_{0.9}As$ active layer.

Then, four high-power 780 nm AlGaAs lasers with selectively buried ridge waveguide (SBR) structures [10] were fabricated to observe the effect of defect engineering on the laser performance, under different growth rates of 7 and 10 Å/s for $Al_{0.1}Ga_{0.9}As$ active layers and under different doping concentrations of 7×10^{-17} cm^{-3} and 1.5×10^{-17} cm^{-3} for p-type $Al_{0.48}Ga_{0.52}As$ cladding layers, as described in Table 2. In the growth of the laser structure, growth conditions for sample #103 were applied to the $Al_{0.48}Ga_{0.52}As$ cladding layers and the p-type doping effects under different growth rates to the $Al_{0.1}Ga_{0.9}As$ active layers. The AlGaAs lasers consisted of a 0.5 μm-thick n-GaAs buffer layer, a 0.2 μm -thick intermediate layer, a 2.5 μm -thick n-AlGaAs cladding layer, three $Al_{0.1}Ga_{0.9}As$ multiple quantum well (MQW) layer, a 0.1 μm-thick etch-stop layer, a 2.2 μm-thick p-AlGaAs cladding layer, a 0.7 μm-thick n-AlGaAs current blocking layer, and a 3.0 μm-thick p-GaAs cap layer from the bottom. The cavity length was 600 μm and the reflectance of the front and rear facets were 10% and 95%, respectively.

Typical values for the current–voltage (I–V) and light output power–current (L–I) characteristics for the four lasers (#107, #108, #109, #110) are summarized in Table 3. By comparison, sample #110 showed the lowest threshold current of 38 mA and the operating current of 129.6 mA at 100 mW with the largest slope efficiency of 1.1 W/A, although the operating voltage of 2.193 V was somewhat higher than those of the others. The relatively higher threshold- and operating-voltage were thought to be due to the lower doping concentrations of the $Al_{0.48}Ga_{0.52}As$ cladding layers. Interestingly, regardless of p-doping for cladding layers, samples #109 and #110 grown at a rate of 10 Å/s

Table 1 Activation energy E_a and trap density N_t calculated for each $Al_{0.48}Ga_{0.52}As$ cladding and $Al_{0.1}Ga_{0.9}As$ active layer

Sample	# 101	# 102	# 103	# 104	# 105	# 106
Grow temperature (°C)	740	740	790	790	790	790
AsH_3 flow (sccm)	300	500	300	500	300	300
Growth rate (Å/s)	12	12	12	12	7	10
E_a (eV)	0.88	0.61	0.58	0.63	0.30 & 0.59 & 1.0	0.30 & 0.61 & 1.01
N_t (10^{15} cm^{-3})	3.85	3.85	3.35	4.25	5.75 & 6.25 & 6.10	2.50 & 5.00 & 3.35

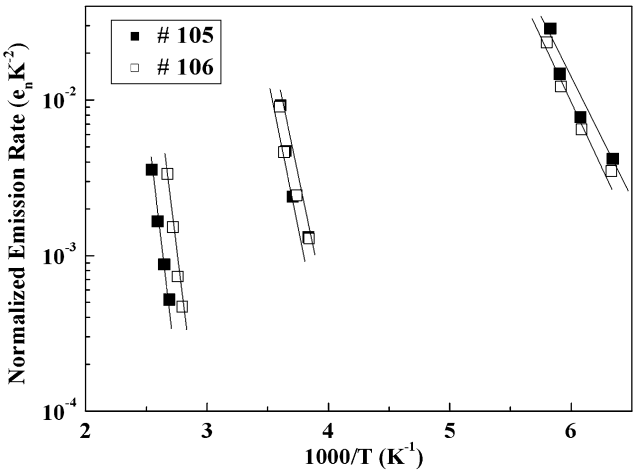

Fig. 4 Arrhenius plots observed from two $Al_{0.1}Ga_{0.9}As$ active layers

Table 2 Growth parameters used for the high-power AlGaAs lasers

Sample	Growth rate for active layers (Å/s)	P-type doping for cladding layers (10^{17} cm^{-3})
# 107	7	7
# 108	7	1.5
# 109	10	7
# 110	10	1.5

Table 3 Comparison of the performances of the four high-power AlGaAs lasers

Sample	V_{th} (V)	I_{th} (mA)	V_{op} (V)	I_{op} (mA)	COD (mA)
# 107	1.794	41.9	2.095	133.1	241
# 108	1.791	40.5	2.187	137.0	239
# 109	1.784	39.7	2.049	138.6	246
# 110	1.798	38.0	2.193	129.6	250

demonstrated better performance than samples #107 and #108 grown at a rate of 7 Å/s; this was consistent with the DLTS result on the $Al_{0.1}Ga_{0.9}As$ active layers. It seems that growth rates have more influence on laser performance rather p-doping for cladding layers under this growth condition. Typical *I–V* and *L–I* curves for sample #110 are represented in Fig. 5. The maximum output power was observed up to 250 mW without any kink at RT. This is the highest output power among 780 nm band lasers reported so far under CW operation to our knowledge. The far-field radiation patterns were measured for mode analyses as shown in Fig. 6. The stable fundamental transverse mode was observed at the power level of 100 mW. The beam divergences perpendicular and parallel to the junction plane were 14 and 7.8 °, respectively. The lasing spectrum taken at

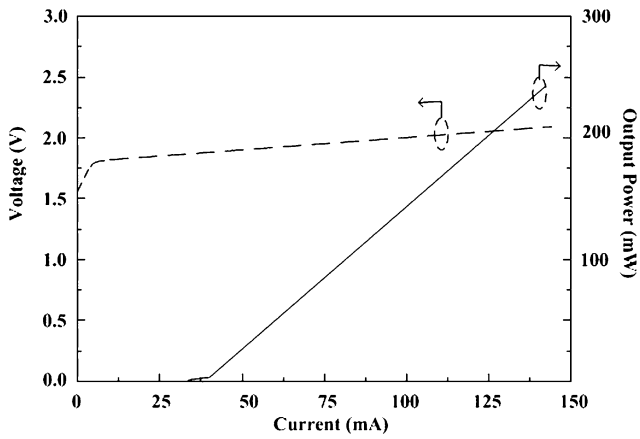

Fig. 5 *I–V* and *L–I* characteristics for the AlGaAs high-power laser under RT CW operation

100 mW is also shown in Fig. 7. Very sharp spectrum was observed at a wavelength of 782.5 nm without any spectral degradation. We contribute this improvement to the structure optimization of the laser by defect engineering through the DLTS analyses.

Conclusion

The growth condition for high-power and high-reliability 780-nm-band AlGaAs LDs was optimized through DLTS analyses by minimizing the trap density of the active and cladding layers of the laser. Then, four high-power 780 nm AlGaAs lasers were fabricated based on the DLTS result and investigated to confirm the effect of defect engineering on laser

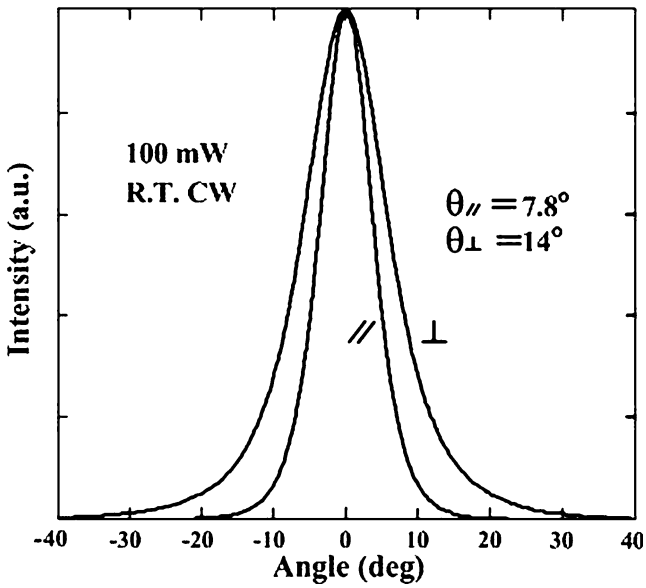

Fig. 6 Far-field patterns taken at 100 mW under RT CW operation

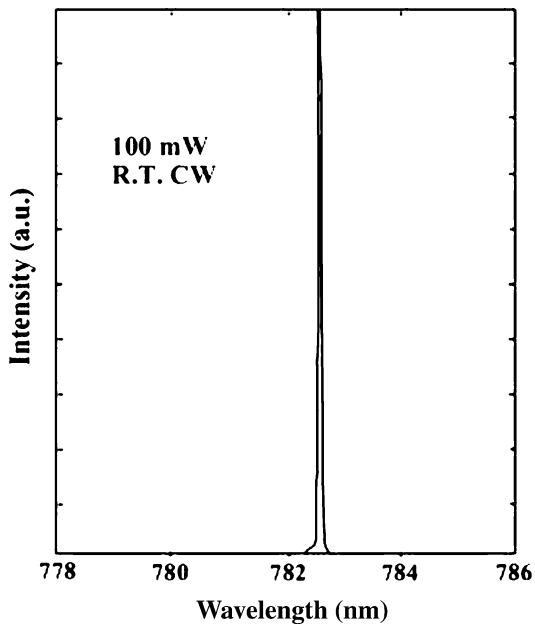

Fig. 7 Emission spectrum taken at 100 mW under RT CW operation

performance. One of the optimized lasers showed improved performance: threshold current of 38 mA, a slope efficiency of 1.1 W/A, and a COD power of 250 mW under RT CW operation. This improvement verified the effectiveness of defect engineering.

Acknowledgement This work was supported by KOSEF through q-*Psi* at Hanyang Univ.

References

1. Tihanyi PL, Jain FC, Robinson MJ, Dixon JE, Williams JE, Meehan K, Heath LS, Beyea DM (1994) IEEE Photo Tech Lett 6:775
2. Yonezu H, Ueno M, Kamejima T, Hayashi I (1979) IEEE J Quan Electron 15:775
3. Hamda K, Wada M, Shimizuk H, Kune M, Susa F, Shibutani T, Yoshikawa N, Kano G, Teramoto I (1985) IEEE J Quan Electron 21:623
4. Shima A, Matsubara H, Susaki W (1990) IEEE J Quan Electron 26:1864
5. Ishii H, Shinagawa T, Tanaka S, Okumura T (2000) J Cryst Growth 210:242
6. Lang DV (1974) J Appl Phys 45:3023
7. Ajjel R, Bouzrara L, Zaidi MA, Maaref H, Bremond G (2003) Physica B 323:15
8. Wagner EE, Mars DE, Hom G, Stringfellow GB (1980) J Appl Phys 51:5434
9. Sakamoto M, Okada T, Mori Y (1985) J Appl Phys 58:337
10. Shima A, Kizuki H, Takemoto H, Karakida S, Miyashita M, Nagai Y, Kamizato T, Shigihara K, Adachi A, Omura E, Otsubo M (1995) IEEE J Select Topics Quantum Electron 1:102